Tissue-embedded CD4$^+$ plasticity structures mucosal immunity in IBD-related inflammation

Qinyue Jiang[1], Veerle Merkus[2], Ciska Lindelauf[1], Nannan Guo[3], Laura F. Ouboter[1,4], Thomas Höllt[5], Caroline R. Meijer- Boekel[6], Frits Koning[1], Andrea E. van der Meulen – de Jong[4], Maria Fernanda Pascutti[1], Vincent van Unen[1]

[1]Department of Immunology, Leiden University Medical Center, Leiden, the Netherlands

[2]Department of Dermatology, Leiden University Medical Center, Leiden, the Netherlands

[3]Microbiome Medicine Center, Department of Laboratory Medicine, Zhujiang Hospital, Southern Medical University, Guangzhou, China

[4]Department of Gastroenterology and Hepatology, Leiden University Medical Center, Leiden, the Netherlands

[5]Computer Graphics and Visualization Group, Delft University of Technology, Delft, the Netherlands

[6]Department of Pediatrics, Leiden University Medical Center, Leiden, the Netherlands

Correspondence:

Vincent van Unen: v.van_unen@lumc.nl

Abstract

Aberrant $CD4^+$ T helper (Th) cell responses to commensal microbiota are implicated in Inflammatory Bowel Disease (IBD), yet the phenotypic states of human tissue Th cells, their differentiation trajectories across active inflammation and remission, and their coordination with other lymphocytes remain poorly defined. Prior work has emphasized peripheral blood or murine models, leaving a gap in how plastic Th programs coexist and evolve in the human intestinal niche in IBD.

We profiled $CD4^+$ T cells from ileocolonoscopic biopsies and paired blood of IBD patients and non-IBD controls, combining spectral flow cytometry with functional assays and histology to map subset composition, activation, and spatial relationships across disease activity states. Here we show that IBD exhibits a dynamic, tissue-embedded $CD4^+$ landscape, characterized by inflammatory expansion, regulatory-Th17 plasticity, branched trajectories toward regulatory and resident fates, coordinated CD4-CD8 networks, and context-dependent cytokine suppression, collectively shaping aberrant mucosal immunity.

Specifically, inflamed mucosa harbored a marked expansion of $CD4^+$ T cells that contracted in remission. Unbiased t-SNE-based analysis revealed several Th populations and linked a $ROR\gamma t^+$ compartment with enhanced T-bet expression to the progression of inflammation. $Foxp3^+$ cells co-expressing RORγt also emerged within the inflamed niche, indicating regulatory-Th17 plasticity. Trajectory visualization revealed a potential branched differentiation path towards either a regulatory phenotype or a tissue-resident phenotype, with both termini expressing activation/proliferation markers. Correlation network analysis connected pro-inflammatory $CD4^+$ states to $T\text{-}bet^+$ and $Granzyme\text{-}B^+$ $CD8^+$ subsets, indicative of crosstalk between helper and cytotoxic lineages. Histology corroborated this organization, showing frequent interactions between $CD4^+$ and $CD8^+$ tissue-resident cells in the lamina propria and epithelial border. In functional assays, TCR stimulation during active disease revealed broad suppression of $CD4^+$ pro-inflammatory cytokines concomitant with expansion of $Foxp3^+$ regulatory T cells. Conversely, a memory Th subset co-expressing HLA-DR and CD38 retained multifunctionality, producing elevated levels of IFNγ, IL-21, IL-22 and IL-10.

Together, these results provide insight into how regulatory-effector plasticity, tissue residency, and CD4-CD8 coordination structure the human intestinal immune landscape in IBD, providing a rational

for therapies to rebalance resident and regulatory programs while preserving beneficial memory responses.

Keywords

IBD; T helper cells; Plasticity; Tissue-resident cells; Mucosal immunology

Introduction

Disrupted immune responses to the gut microbiota in genetically susceptible individuals, potentially triggered by largely unknown environmental factors, contribute to the pathogenesis of Inflammatory Bowel Diseases (IBD)[1, 2]. IBD typically follows a chronic, relapsing-remitting course, and comprises two main subtypes: Crohn's disease (CD) and ulcerative colitis (UC). UC affects the colon and is characterized by continuous mucosal lesions, whereas CD can involve any segment of the gastrointestinal tract and frequently displays transmural inflammation. Current therapeutic goals are to induce and maintain clinical, biochemical, and durable endoscopic remission to minimize bowel damage and improve long-term outcome[3]. Neither CD nor UC has a single phenotype; both are heterogeneous with respect to clinical presentation, treatment responses, and immune profiles[4]. Management of disease remains largely reactive, with treatment adjustments commonly driven by worsening of clinical parameters. Molecular and cellular characterization that accounts for inter-individual variability in tissue pathology could better guide clinical management and advance personalized therapy in IBD[5]. Dysregulation and function of $CD4^+$ T cell subsets are widely implicated in chronic intestinal inflammation. In IBD, an imbalance between inflammation-promoting and immunoregulatory populations sustains mucosal damage and persistent immune activation, ultimately contributing to the development of chronic disease[6]. Upon antigen recognition, naive $CD4^+$ T cells can differentiate into distinct effector subsets, including pro-inflammatory Th1, Th2, and Th17, as well as a regulatory T (Treg) subset [7, 8]. In the intestine, regional tissue-resident memory $CD4^+$ T cells (T_{RM}) provide long-term local immunity to microbial antigens, and can be rapidly reactivated, undergo transient proliferation, and reacquire distinct T-helper phenotypes[9]. Recent studies highlighted that polarized T-helper cells can adopt alternative phenotypes and functionalities during disease progression, accompanied by changes in signature transcription factors and lineage-defining cytokine

profiles[10-12]. While bidirectional Treg–Th17 plasticity has been described in IBD [11, 12], the mechanisms governing this switching in human intestinal tissues across disease states remain poorly defined.

Although $CD4^+$ T cells are major contributors to chronic intestinal inflammation, the intestinal immune landscape includes diverse cell types that interact with $CD4^+$ T cells across the lamina propria and intraepithelial compartments to shape adaptive responses in IBD. Among these, $CD8^+$ T cells, located in proximity to $CD4^+$ T cells, are thought to be implicated in epithelial injury in IBD[13-15]. We previously identified an inflammation-associated immune network enriched for activated HLA-DR^+CD38^+ effector memory $CD4^+$ T cells in treatment-naive IBD patients[16]. However, the phenotype, function, and trajectory of this population, particularly during disease remission, remain poorly defined.

To address these gaps, we performed immunological functional assays with spectral flow cytometry on freshly obtained intestinal biopsies and paired peripheral blood from patients with active IBD or in clinical remission, as well as non-IBD noninflamed controls. Here, we show that IBD harbors a dynamic, tissue-embedded $CD4^+$ landscape with inflammatory expansion that recedes in remission, regulatory–Th17 plasticity (Foxp3–RORγt), and branched trajectories toward regulatory and tissue-resident fates. We also show coordinated CD4–CD8 networks and a multifunctional HLA-DR^+CD38^+ memory subset that persists despite global cytokine suppression, pointing to the development of rational therapeutic strategies to rebalance resident/regulatory programs while preserving protective memory.

Results

$CD4^+$ T cells are enriched in the inflamed mucosa

To comprehensively assess intestinal and circulating T cells, together with other conventional and non-conventional lymphoid subsets, we applied a validated 37-plex full spectral flow cytometric panel[5] to single-cell suspensions of endoscopic intestinal samples (n=68) and peripheral blood mononuclear cells (PBMCs) (n=32) from 27 IBD patients (CD, n=17; UC, n=10) and 5 controls (clinical metadata listed in Supplementary Table 4), yielding a dataset on 3.5 million live $CD45^+$ cells (Supplementary Fig. 1A). Based on marker expression profiles, we delineated the intestinal T cell compartment and identified 7 major subsets: $CD4^+$ T cells, conventional $CD8\alpha\beta^+$ T cells, $CD8\alpha\alpha^+$ T cells, $CD8\alpha\beta^+$ NKT cells, double-negative (DN) T cells ($CD8\alpha^-CD8\beta^-CD4^-$), mucosal-associated invariant T (MAIT) cells, and γδ T cells

(Fig. 1A). Next, samples were stratified by disease status (control, noninflamed, inflamed and remission), disease subgroup (control, CD, UC), and intestinal location of the analyzed samples (colon and ileum) (Fig. 1B). Cell-frequency analysis revealed pronounced heterogeneity in immune composition, with $CD4^+$ T cell subsets predominating in the inflamed mucosa (Fig. 1B). Density plots of an opt-SNE analysis s highlight differential presence of the $CD4^+$ T cell subsets depending on disease status (Fig. 1C and Supplementary Fig. 1B). Consistently, $CD4^+$ T cells were significantly upregulated during inflammation and downregulated in remission across disease types (CD, UC) and sites (colon, ileum) (Fig. 1D). In contrast, the other major lineages declined (conventional $CD8\alpha\beta^+$ T, NKT and γδT cells) or remained unchanged ($CD8\alpha\alpha^+$ T, DN and MAIT cells) (Supplementary Fig. 1C) in the inflamed mucosa.

Inflammation shapes the $CD4^+$ memory T cell landscape

Next, we performed a t-SNE analysis of the $CD45RA^+CCR7^-$, $CD45RA^-CCR7^-$, and $CD45RA^-CCR7^+$ $CD4^+$ memory T cells (T_M). Based on the marker expression profiles, hierarchical clustering of the collective 65,732 cells yielded 46 distinct T_M-helper clusters (Fig. 2A-B and Supplementary Fig. 2A). The associated density plots display diverse distribution patterns that are associated with disease state (Fig. 2B). Pearson's rank correlation analysis identified four main cellular networks (Supplementary Fig. 2B), of which two (Fig. 2C) correspond to the high-density regions of the noninflamed and inflamed groups shown in Fig. 2B, respectively. By analyzing the frequencies of those clusters, we observed that CD4-15, CD4-12 and CD4-48 were underrepresented during the active phase of disease (Fig. 2D), while CD4-13, CD4-5, CD4-7, CD4-18, CD4-21 and CD4-4 were notably increased in the inflamed group and decreased following the resolution of inflammation (Fig. 2E). The remaining clusters showed no significant quantitative changes.

To refine the phenotypic features of subsets involved in IBD inflammation, we overlaid marker expression across clusters (Fig. 2F and Supplementary Fig. 2C). Most $CD4^+$ T_M clusters displayed $CD45RA^-CCR7^-$ effector-memory features, whereas a minority within CD4-18 and CD4-21 co-expressed CCR7, consistent with a central memory phenotype (Supplementary Fig. 2C). Compared to naive T cells, all these $CD4^+$ T_M subsets exhibited abundant expression of CD69, indicating tissue-residency. Strikingly, the six inflammation-linked clusters (CD4-13, CD4-5, CD4-7, CD4-18, CD4-21, and CD4-4) co-expressed HLA-DR, CD38, and CD39 to varying degrees, consistent with activation. In addition, the expression of

Ki-67 in CD4-5, CD4-7 and CD4-18 suggested proliferative potential. Distinct expression patterns of the transcription factors (T-bet, RORγt, Foxp3 and Helios) were observed among the $CD4^+$ T_M clusters. For example, CD4-5 and CD4-7 co-expressed RORγt and T-bet and were otherwise phenotypically similar, differing primarily by CD103 expression restricted to CD4-7, consistent with Th1/Th17-like states distinguished by the tissue-residency integrin CD103. Moreover, inflammation-associated CD4-18, CD4-21 and CD4-4 expressed Foxp3, with variable RORγt and Helios, indicating Treg identity and plasticity. Furthermore, we performed PCA on frequencies of 46 $CD4^+$ T_M cell clusters (Supplementary Fig. 2D). Noninflamed samples (control, noninflamed IBD and remission) were clustered together and apart from inflamed samples. CD and UC samples were separated from the controls, with clear colon-ileum stratification. Overall, the inflammatory status was the dominant source of variation. .

Collectively, these findings suggest a disease-state–dependent, tissue-resident $CD4^+$ memory landscape, with heterogeneous Th1/Th17 and $Foxp3^+$ networks, whose frequencies stratify colon *versus* ileum and IBD *versus* control, increase with inflammation, and recede in remission.

Trajectory analysis reveals bifurcating inflammatory paths of $CD4^+$ memory T cell differentiation

Given the observed plasticity within $CD4^+$ T-helper subsets, we next examined how these states evolve during inflammation. We used the dynamic t-SNE visualization in Cytosplore with naive $CD4^+$ T cells as a reference (Fig. 3A and Supplementary Fig. 3A) [17, 18]. Cells were initially unordered at onset of the t-SNE computation, but by stage 2 naive cells segragated from the remainder memory cells. By stages 3–4 an interconnected network emerged with two branches bridged by cluster 13 (Fig. 3A). Disease-status overlays showed that the left branch comprised noninflamed clusters (CD4-12, CD4-15, CD4-48), whereas the right branch contained inflammation-linked clusters (CD4-5, CD4-7, CD4-4, CD4-18, CD4-21) (Fig. 3B). Marker expression profiles showed CD127 enrichment along the noninflamed branch and uniform CD39 positivity across inflamed clusters, with concurrent increases in CD38, HLA-DR and Ki-67 on the inflamed branch (Fig. 3C), consistent with activation and proliferation.

To quantify marker dynamics along putative differentiation pathways, we applied Wishbone rooted at the intermediate cluster 13. This analysis revealed a clear bifurcation driven by divergent expression of RORγt/CD103 *versus* Foxp3/CTLA-4/CD25/Helios (Fig. 3D-E), delineating inflammatory trajectories

toward a tissue-resident Th17-like fate (Branch I) and a regulatory fate (Branch II), respectively. Activation markers (HLA-DR, CD38, CD39, Ki-67) rose along the inflamed branch, supporting a model of inflammation-associated maturation from a shared intermediate. Additional overlays further corroborated branch identity (Fig. 3C-E): CD161 and CCR6-canonical Th17 features were concentrated along the inflamed, tissue-resident branch (Branch I), whereas CCR4 and CD27, characteristic of Treg/less-differentiated memory, were biased toward the inflamed, regulatory branch (Branch II). CXCR3 aligned with T-bet–associated segments within Branch I, CD69 was broadly elevated across both branches, and a small $CD56^+$ subset localized in the noninflamed branch, suggesting NK-like attributes.

Taken together, these analyses reveal a bifurcation from a shared intermediate into two inflammatory trajectories; one toward a tissue-resident Th17-like effector state and the other toward a regulatory fate, signifying inflammation-driven diversification of $CD4^+$ T-helper memory programs

Coordination of $CD4^+$ and $CD8^+$ T-cell programs at the mucosal interface in IBD

To interrogate potential CD4–CD8 crosstalk in the intestine, we next characterized the $CD8^+$ T-cell compartment. Unsupervised dimensionality reduction identified 20 phenotypically distinct $CD8^+$ clusters (Supplementary Fig. 4A). We then integrated these $CD8^+$ clusters with the $CD4^+$ memory clusters and performed a Pearson correlation network analysis, resolving five multi-lineage cellular networks (Fig. 4A), characterized by strong within-network positive correlations and between-network anticorrelations. Network 3 contained the five inflammation-associated $CD4^+$ clusters (CD4-4, CD4-5, CD4-7, CD4-18, CD4-21) together with five $CD8^+$ clusters (CD8-2, CD8-3, CD8-8, CD8-9, CD8-10). Four of the five $CD8^+$ clusters displayed a $CCR7^-CD45RO^+CD45RA^+$ effector-memory phenotype, whereas CD8-3 was $CCR7^-CD45RO^-CD45RA^+$, consistent with a terminally differentiated (T_{EMRA}-like) state (Fig. 4B; Supplementary Fig. 4B). CD8-3, CD8-8, and CD8-9 showed a conventional CD8αβ phenotype; clusters 8 and 9 expressed Granzyme-B, indicating cytolytic potential, and CD8-9 additionally expressed CD103, consistent with tissue residency. In contrast, CD8-2 and CD8-10 lacked CD8β and co-expressed CD4 with CD8α, alongside RORγt and T-bet (Fig. 4C; Supplementary Fig. 4B). Notably, all five $CD8^+$ clusters were significantly increased, or trended upward, in inflamed samples in parallel with their correlated $CD4^+$ memory clusters (Fig. 4D). Conversely, four $CD8^+$ clusters were reduced in inflammation (Supplementary Fig. 4C), indicating contraction of noninflamed/homeostatic states outside Network 3.

To define the spatial organization of resident $CD4^+$ and $CD8^+$ T cells in the inflammatory microenvironment, we performed six-color multispectral immunofluorescence on inflamed colonic tissue from patients with CD (n=2) and UC (n=3), as well as on noninflamed colonic tissue from healthy donors (n=2), displaying four representative regions of interest (ROIs) per group. We simultaneously detected E-cadherin, CD3, CD4, CD8, CD103, and DAPI (Fig. 4E). Compared with controls, IBD samples showed increased T-cell infiltration within the lamina propria and along the epithelial interface, with frequent juxtaposition of $CD4^+$ and $CD8^+$ cells (white arrows). $CD103^+$ intraepithelial cells were predominantly $CD8^+$ (yellow arrows), whereas $CD103^+CD4^+$ cells localized near the epithelial border or within the lamina propria (magenta arrows), consistent with coordinated resident programs at the mucosal interface. Notably, this spatial pattern accords with the trajectory analysis (Fig. 3), which revealed progressive CD103 induction along the inflammatory $CD4^+$ branch, linking residency programming to epithelial-proximal positioning.

Inflammation dampens TCR-mediated activation of $CD4^+$ memory T Cells

To assess $CD4^+$ T cell function, we stimulated single-cell suspensions from intestinal biopsies with α-CD3/α-CD28 for 6 hours and profiled CD40L together with cytokines characteristic of Th1 (IL-2, TNFα IFNγ), Th2 (IL-13, IL-4), Th17 (IL-17A, IL-21, IL-22), and Treg (IL-10) by spectral flow cytometry (Supplementary Fig. 5A). Noninflamed samples (controls, noninflamed IBD, remission) were pooled and compared with inflamed samples. Two experimental batches showed concordant trends and are presented separately in Supplementary Fig. 5B-C, and the combined cohort is shown in Figure 5.

CD40L was robustly induced by stimulation in all groups but rose less in inflamed tissue, indicating attenuated activation (Fig. 5A). $HLA\text{-}DR^+CD38^+$ $CD4^+$ T_M cells were higher at baseline in inflamed mucosa and remained at similar frequencies after stimulation (Fig. 5B). By contrast, $CXCL13^+CD4^+$ T_M cells were mostly reduced in inflamed samples after stimulation (Fig. 5C)

We next quantified cytokine production within the memory compartment (Fig. 5D-E and Supplementary Fig. 5C). After 6 hours, Th1 cytokines (IL-2, TNFα, IFNγ) predominated, Th17 cytokines (IL-17A, IL-21, IL-22) were lower in abundance, and Th2/Treg cytokines (IL-13, IL-4, IL-10) were largely rare. Moreover, TNFα was significantly decreased in the inflamed group, with IL-2 and IFN-γ showing only mild reductions; these differences persisted when gating on activated $CD40L^+$ cells (Fig. 5E). IL-

17A, and IL-21 were largely unchanged, while IL-22 trended lower. IL-13/IL-4 showed a small but statistically significant difference with low absolute frequencies, and IL-10 showed no clear change (Fig. 5D).

To investigate mechanisms of reduced cytokine production, we related Foxp3$^-$ effector output to Foxp3$^+$ Treg abundance. Significant negative correlations with Foxp3$^+$ frequency were observed for IFNγ and IL-17A, with a trend for TNFα (Fig. 5F). Th2 cytokines and IL-10 were not significantly correlated. In addition, a multifunctional subset co-producing IL-2, TNFα and IFNγ was likewise diminished in inflamed tissue upon stimulation and inversely associated with Foxp3$^+$ frequency (Fig. 5G-H).

Applying the same stimulation to paired blood samples revealed comparable CD40L induction and cytokine production between inflamed and noninflamed groups (Supplementary Fig. 6), suggesting that the hypo-responsiveness is tissue-localized. Collectively, despite intact proximal activation, memory CD4$^+$ T cells from inflamed mucosa display selectively blunted Th1 effector function and reduced multifunctionality, features that are tissue-localized and in part linked to increased regulatory burden.

HLA-DR$^+$CD38$^+$ memory CD4$^+$ T cells are enriched in IBD and display an activated, tissue-resident, proliferative, and multifunctional profile

We previously noted an expansion of activated HLA-DR$^+$CD38$^+$ effector-memory CD4$^+$ T cells in treatment-naive IBD[16]. Here, including both active disease and remission, we confirmed that HLA-DR and CD38 are upregulated across central memory (T_{CM}), effector memory (T_{EM}) and terminally differentiated effector memory (T_{EMRA}) subsets (Fig. 6A), and that the HLA-DR$^+$CD38$^+$ fraction is increased in inflamed tissue and reduced in remission (Fig. 6B).

Analysis of the transcription factor composition demonstrates that within HLA-DR$^+$CD38$^+$ memory cells, a large subset (~25%) was negative for the lineage factors T-bet, RORγt and Foxp3, with single-positive Foxp3$^+$ cells comprising a minority (~10%) (Fig. 6C). Nonetheless, RORγt expression was clearly enriched (~23%) and included a subset co-expressing T-bet (~20%). Foxp3 and Helios were present at lower but increased levels relative to HLA-DR$^-$CD38$^-$ cells (Supplementary Fig. 7A-C).

Next, we compared the phenotypic profiles among HLA-DR/CD38-defined memory subsets within inflamed tissue. Compared with HLA-DR^{-}CD38^{-} memory cells, HLA-DR^{+}CD38^{+} population showed higher CD25 and lower CD127 (Fig. 6D), indicating enhanced IL-2 receptor signalling and recent activation. They also upregulated CTLA-4 and CD39 (Fig. 6E), consistent with engagement of regulatory pathways and ectonucleotides activity that can generate immunomodulatory adenosine. The same cells expressed increased CD103 and CD69 (Fig. 6F), markers of tissue residency and epithelial retention, and exhibited elevated Ki-67 (Fig. 6G), indicating ongoing proliferation. Finally, T-bet and RORγt were enriched in the HLA-DR^{+}CD38^{+} subset (Fig. 6H), supporting polarization toward Th1/Th17 programs. Cells single-positive for HLA-DR or CD38 generally displayed intermediate levels across these features (Fig. 6D–H), placing them between quiescent double-negative and fully activated double-positive states.

Finally, we assessed cytokine production by HLA-DR^{+}CD38^{+} CD4 T_M cells. Upon stimulation with α-CD3/ α-CD28, this subset produced more IFNγ, IL-21, IL-22, IL-10 than HLA-DR^{-}CD38^{-} counterparts (Fig. 6I). In contrast, IL-2, TNFα and Th2 cytokines (IL-13/IL-4) were comparable between groups (Fig. 6I), pointing to selective multifunctionality. Taken together with their activation, residency, and proliferative features, these data position HLA-DR^{+}CD38^{+} CD4^{+} memory cells as tissue-embedded effectors that can both amplify inflammation and modulate it through targeted cytokine programs.

Discussion

Our finding delineate how inflammatory cues reshape the intestinal T cell landscape in IBD, with implications for patient heterogeneity and therapy response. In active IBD, we observed a pronounced expansion of activated CD4^{+} memory T cells, marked by upregulation of HLA-DR and CD38, alongside contraction of other T cell subsets in the mucosa. These inflammation-associated CD4^{+} T cells displayed a tissue-resident profile (CD69, CD103) and elevated proliferation, indicating their persistence at the disease site. Notably, their abundance dropped once inflammation resolved (remission), highlighting a reversible, state-dependent T cell reprogramming. Such cells were often juxtaposed with CD8^{+} T cells at the epithelial interface, suggesting coordinated mucosal immune responses. Functionally, we found these CD4^{+} T cells in inflamed tissue to be hyporesponsive. Upon TCR stimulation (α-CD3/ α-CD28) they produced lower levels of key effector cytokines (especially TNFα and IFNγ) and showed reduced

polyfunctionality. This intriguing dampening of effector function occurred despite their activated phenotype, and we found it to be inversely correlated with local Foxp3$^+$ Treg cell abundance. In essence, active IBD lesions are characterized by a paradoxical mix of highly activated yet functionally restrained CD4$^+$ T cells, likely reflecting a dominant regulatory influence or incipient T cell exhaustion in the chronic inflammatory milieu. Together, these results define a distinctive inflammation-associated CD4$^+$ T cell signature in IBD and underscore the dynamic plasticity of mucosal T cells; changes that may underlie the variability in clinical outcomes and therapeutic responses among patients.

In mapping the intestinal lymphocyte compartment, our high-dimensional approach also captured several 'unconventional' T-cell subsets (γδ T cells, MAIT cells and NKT-like cells) beyond the classical αβ T cells[19, 20]. We noted significant differences in these cells during inflammation. γδ T cells, which normally reside abundantly in intestinal epithelium, were markedly decreased in the inflamed mucosa in our IBD cohort. This aligns with some reports that mucosal γδ T cells are perturbed in IBD, although findings have varied[21]. For example, a shift in γδ T cell subsets was observed with Vδ1 cells (normally dominant in healthy colon) being reduced and pro-inflammatory Vδ2 cells enriched in chronic IBD lesions, producing excess IFNγ, TNFα and IL-17[22]. In contrast, a recent study identified a tissue-protective subset of CD103$^+$Vγ4$^+$ intraepithelial γδ T cell that was selectively lost in IBD, and whose restoration correlated with disease remission[23]. These findings underscore a dual role for γδ T cells in IBD: certain subsets may promote inflammation while others maintain barrier integrity, and inflammation skews this balance. Invariant NKT cells (CD1d-restricted T cells) were also diminished in our inflamed samples. Consistently, clinical studies have reported that type 1 NKT cells are reduced in the blood and intestine of CD and UC patients, whereas type 2 NKT cells can accumulate in UC lamina propria, potentially contributing to a typical Th2 responses[24]. MAIT cells, which respond to bacterial metabolites, showed no significant frequency change in our dataset (likely due to their low baseline numbers). However, literature suggests MAIT cells redistribute in IBD; they diminish in circulation but can accumulate in inflamed gut tissue[25]. We did not further dissect these non-conventional T-cell subsets or their potential crosstalk with CD4$^+$ T cells. Nonetheless, our observations of decreased γδ T and NKT cells in active IBD reinforce the idea that intestinal inflammation can differentially affect innate-like T-cell populations.

Intriguingly, parallel analysis of patient blood did not reveal dramatic differences in major T cell subsets

between active disease and remission. This suggests that systemic immune profiles may remain relatively steady and highlights the compartmentalized nature of IBD inflammation. It also underlines that therapies aiming to normalize the intestinal immune niche should focus on the tissue-resident cells.

Within the gut, a key finding of our study is the plasticity of $CD4^+$ T-helper cells under inflammatory conditions. We identified 'formerly' Th17 cells that had acquired mixed phenotypes, some co-expressing T-bet and producing IFNγ (Th1-like), others upregulating Foxp3 and CTLA-4 (Treg-like), indicating divergent differentiation in response to the IBD environment. The transcriptional program of Th17 cells, governed by RORγt, is known to endow these cells with remarkable flexibility, enabling them to adopt alternate fates depending on context. Environmental cues in the intestinal mucosa, such as cytokines, microbiota-derived products, and metabolic factors, can thus redirect Th17 cells towards either pathogenic or regulatory trajectories[26]**.** This concept of Th17 cell plasticity has gained traction as a unifying mechanism in chronic inflammation. For instance, Th17 cells can convert into IFNγ-producing Th1-like cells ('ex-Th17' cells) or into IL-10-producing Treg-like cells, blurring traditional T-helper lineage boundaries[27]. In IBD, both Th1 and Th17 responses are elevated, and indeed we and others find cells producing IFNγ and IL-17 in inflamed mucosa[28]. These cells likely represent Th17 cells transitioning toward a Th1 phenotype. Notably, IL-23, a cytokine abundant in IBD mucosa, appears to be a key driver of this conversion. IL-23 can shift Th17 cells into an IFNγ–high, IL-17–low state, effectively generating Th1-like cells from Th17 precursors[28]. It does so by inducing STAT4/T-bet pathways while suppressing TGFβ-driven IL-17 production. Consistent with this, blocking IL-23 in murine colitis prevents the emergence of $IFN\gamma^+IL\text{-}17^+$ mixed cells and ameliorates disease Clinically, therapies targeting the IL-23/Th17 axis have shown remarkable efficacy in IBD. Ustekinumab (anti-p40, blocking IL-12 and IL-23) and newer IL-23p19 inhibitors have achieved high remission rates in patients [29, 30], whereas direct IL-17A neutralization surprisingly failed or even worsened disease outcomes[31]. One explanation is that IL-17 plays a dual role: it contributes to inflammation but also is essential for mucosal barrier defense and tissue repair[32]. Blocking IL-17 deprives the host of a key protective factor, leading to infection and impaired healing; an insight that explains why IL-23 (upstream in the Th17 pathway) is a safer therapeutic target. By modulating Th17 plasticity rather than abrogating IL-17 entirely, IL-23 blockade may tilt the balance back towards regulation without compromising barrier

integrity. Our data provide a cellular basis for these observations: during active inflammation, Th17-lineage cells bifurcate into pro-inflammatory tissue-resident (Th1-like) and anti-inflammatory (Treg-like) subsets, and successful therapy likely requires damping the former while boosting the latter.

In light of the above, the interplay between Th17 cells and Foxp3$^+$ Treg cells emerges as a central theme in IBD immunopathology. We observed that several inflammation-associated CD4$^+$ T cell clusters co-expressed RORγt and Foxp3, or upregulated regulatory molecules (CTLA-4, CD39) despite being in an active disease setting. This raises the possibility that some Th17 cells are transitioning into regulatory cells *in situ*. In chronic or resolving inflammation, it has been reported that some Th17 cells can downregulate RORγt and convert into Foxp3$^+$ Tregs, a phenomenon first demonstrated in a fate-mapping study by Gagliani *et al.* in an intestinal inflammation model[33]. These "ex-Th17" regulatory cells (often IL-10$^+$ and Foxp3$^+$) may serve to counteract inflammation as a negative feedback mechanism. Our trajectory analysis supports a similar Th17-Treg branch, wherein an intermediate Th17-like population potentially gives rise to a Foxp3$^+$ subset under inflammatory conditions. We speculate that RORγt$^+$ Th17 cells, after initial pathogenic expansion, may acquire regulatory features (Foxp3, CTLA-4, CD25, CD39) in an attempt to dampen the immune response. This could represent a form of intrinsic regulation that kicks in during chronic inflammation. On the flip side, strong inflammatory signals can destabilize conventional Tregs or impede their function. Cytokines such as IL-6, IL-1β, and IL-23 not only promote Th17 differentiation but can also drive "conversion" of Foxp3$^+$ Tregs into effector T cells. Under highly inflammatory conditions, Foxp3$^+$ Tregs have been shown to lose Foxp3 expression and begin secreting IL-17A and IFN-γ[34]. In our data, the Foxp3$^+$ Tregs in inflamed tissue often co-expressed RORγt, suggesting exposure to Th17-skewing signals. It is conceivable that some of these Foxp3$^+$ cells were originally Tregs that partially de-differentiated or "plasticized" into Th17-like cells early in the inflammatory process. The bidirectional plasticity between Th17 and Treg lineages adds a layer of complexity: the balance of pro- vs. anti-inflammatory CD4$^+$ T cells in IBD may be constantly changing, influenced by local cytokine milieu.

Therapeutically, this underscores the importance of restoring the Th17/Treg balance. One approach is to boost regulatory T cells. Indeed, low-dose IL-2 therapy (which preferentially expands Tregs) has recently been tested in ulcerative colitis. A phase 1b trial reported that low-dose IL-2 was safe and led to expansion of circulating Tregs and clinical improvement in a subset of UC patients [35]. However, given

Tregs' susceptibility to instability, simply increasing their number may not confer lasting benefit unless the inflammatory environment is controlled. Some Tregs might lose Foxp3 in the cytokine-rich gut milieu, as noted above, potentially limiting the efficacy of Treg therapy. Other strategies are being explored; for example, antigen-specific Tregs or CAR-Tregs targeting gut-homing receptors (like IL-23R) to ensure Tregs migrate to and persist in intestinal lesions[36]. Another strategy is concomitant blockade of inflammatory pathways (e.g. IL-6/STAT3) during Treg therapy to prevent Treg-to-Th17 conversion[34].

Taken together, our findings highlight that targeting T-cell plasticity, stabilizing regulatory T cells while dampening pathogenic Th1/Th17 cells, could be a promising therapeutic paradigm. In future studies, it will be valuable to determine definitively (e.g. through lineage tracing in human tissues) whether the Foxp3$^+$RORγt$^+$ cells in IBD are former Th17 cells acquiring suppressive functions or *vice versa.* Such insights would inform therapies to selectively reinforce the endogenous regulatory circuit of the immune system.

We found that a subset of CD4$^+$ T cells in IBD not only takes on an inflammatory phenotype but also upregulates markers of tissue residency. In particular, clusters on the Th17-like inflammatory trajectory increasingly expressed CD69 and CD103, indicating a transition to tissue-resident memory T cells. Tissue-resident T cells reside in the gut mucosa for decades[37], where they can react swiftly to local stimuli. Recent research has begun to delineate the role of tissue-resident memory T cells in IBD. Yokoi *et al.* identified a unique CD103$^+$CD161$^+$CCR5$^+$ CD4$^+$ tissue-resident subset that is highly enriched in Crohn's disease intestinal mucosa[38]. These cells exhibited innate-like effector functions, produced large amounts of IFNγ upon stimulation, and clustered near the epithelium. In our study, the inflammation-linked CD4$^+$ tissue-resident memory cells (exemplified by cluster 7) likely represent the long-lived pathogenic effectors that embed in the gut tissue and could drive disease recurrence or persistence. Their presence might explain why some patients relapse quickly after stopping therapy: a pool of resident memory T cells 'remembers' the inflammatory program and reignites it upon trigger.

Correlation network analysis in our data showed that the inflammation-associated CD4$^+$ clusters were tightly linked to certain CD8$^+$ T-cell clusters (forming a multi-lineage network). These CD8 subsets, which expanded in active disease, included CD8$^+$CD103$^+$ cytotoxic tissue-resident cells and an unconventional CD4$^+$CD8α$^+$ double-positive T cell population co-expressing T-bet and RORγt. Spatially, multiplex immunofluorescence confirmed that inflamed IBD tissues have dense aggregates of CD4$^+$

and $CD8^+$ T cells intermingled in the intestine. $CD8^+$ T cells (especially $CD8\alpha\beta^+CD103^+$ IELs) were observed within or just below the epithelium, often adjacent to $CD4^+$ cells, pointing to possible cross-talk. This coordinated localization suggests a scenario where $CD4^+$ T cells and $CD8^+$ cytotoxic T cells jointly contribute to epithelial injury in IBD. Treatments like vedolizumab (anti-α4β7 integrin) or S1P modulators prevent lymphocyte homing to the gut, which will reduce influx of both $CD4^+$ and $CD8^+$ T cells into the intestine. Indeed, blocking T-cell trafficking has proven effective for IBD, vedolizumab induces remission by selectively keeping T cells out of the gut while preserving systemic immunity[39]. However, resident cells already in the tissue might persist; thus, combining trafficking blockers with strategies to deactivate or reprogram the resident T cells might yield synergy.

Our finding that tissue $CD4^+$ memory T cells in active IBD are hypofunctional (potentially due to regulatory engagement) hints that enhancing local regulatory pathways could further quell inflammation. One could envision approaches to promote tissue-resident regulatory T cells. Another approach is reducing antigenic drive: IBD T cells are stimulated by a complex antigen pool (commensal bacteria, dietary antigens). Therapies that alter the gut microbiome (such as fecal microbiota transplant) or induce tolerance to commensals might decrease the continuous (though as-yet unknown) drivers that keep tissue T cells activated in IBD. While such microbiome-directed strategies are still experimental, they hold the promise of dampening mucosal T-cell activation at the source.

In summary, this study provides an integrated view of how inflammation sculpts the intestinal T-cell compartment in IBD, revealing distinct T-cell states linked to disease activity. We propose that IBD flares are driven by a network of tissue-resident Th17/Th1-skewed $CD4^+$ T cells and cytotoxic $CD8^+$ memory T cells at the mucosal front, whose inflammatory behavior is kept partly in check by an expanding counter-network of regulatory T cells. When inflammation subsides (either naturally or via treatment), this pathogenic network contracts and the regulatory arm regains dominance, restoring homeostasis. Therapeutically, these insights reinforce the notion that precision targeting of T-cell subsets is warranted. Rather than broad immunosuppression, future treatments could aim to: eliminate or reprogram the pathogenic tissue-resident memory T cells, or enhance mucosal regulatory cells.

Our study has limitations that open avenues for further research. We primarily profiled T cells; however, interactions with other immune cells (B cells, macrophages, ILCs) were not directly interrogated here.

Additionally, our data are cross-sectional; longitudinal sampling before, during, and after therapy would be valuable to observe T-cell state transitions and confirm which changes are causes or consequences of healing. Technical aspects like the use of ex vivo stimulation should be expanded with antigen-specific stimulation assays to mimic chronic exposure to microbial antigens. Finally, it would be intriguing to molecularly characterize the epigenetic landscape of these inflammation-adapted T cells

In conclusion, the dynamics of $CD4^+$ T-cell plasticity and CD4–CD8 T-cell cooperation uncovered in this study underscore the adaptive complexity of the mucosal immune system in IBD. By harnessing the accumulating knowledge of T-cell states, pro-inflammatory *versus* regulatory, resident *versus* circulating, stable *versus* plastic, we can move toward therapies that restore immune balance with minimal collateral damage. The ultimate goal will be to achieve durable remission in IBD by extinguishing the pathogenic T-cell memory of inflammation while boosting the mucosal immune regulatory arm. Our results provide a roadmap of cellular targets and interactions to guide this development of novel targeted immunotherapies for IBD.

Materials and Methods

Patients

IBD patients (minimum age 12 years old) were recruited from the Department of Gastroenterology and the pediatric department at Leiden University Medical Center Patients either had a prior diagnosis of IBD or underwent diagnostic ileocolonoscopy based on clinical suspicion of newly onset IBD. Controls were patients $\geq$ 18 years old known with another disease, like colorectal cancer in the past or with familial colon cancer who underwent a surveillance ileocolonoscopy. The studies were reviewed and approved by the Medical Ethical Committee of Leiden University Medical Center. After informed consent, fresh biopsies and peripheral blood were obtained directly at the endoscopy room according to protocol P15.193. Fresh samples were processed (see below) and results were stored in the LUMC-IBD biobank (protocol: B20.004).

The phenotype characterization cohort includes 68 intestinal samples from 27 patients (CD, n=17; UC, n=10) and controls (n=5). For T cell receptor stimulation assay, the primary cohort includes 20 intestinal

samples from 6 IBD patients (CD, n=3; UC, n=3) and 3 controls. The validation cohort included 25 intestinal samples from 10 patients (CD, n=5; UC, n=5) and 4 controls. Samples from 3 of these controls and 7 of these patients (CD, n=3, UC, n=4) were also utilized for phenotypical investigation.

Sample and clinical data collection

The clinical characteristics of all samples are shown in Supplementary Table 4. In IBD patients, samples from rectum, colon and ileum, both from inflamed and endoscopic noninflamed mucosa (if available) were collected. Noninflamed mucosa was labeled as bowel segment never inflamed or bowel segment currently endoscopic remission (previously involved segment). Peripheral blood was drawn from all participants at the time of endoscopy.

Patients were classified according to the Montreal classification regarding age at diagnosis, location / extent of disease and behavior. In CD patients, the inflamed segment of each patient was classified according to the SES-CD, as inactive (0-2), mild (3-6), or moderate-severe (≥7). In UC patients severity of disease was scored according to the endoscopic Mayo score (inactive (0), mild (1) or moderate-severe (2-3).

Isolation of single cells from endoscopic intestine and peripheral blood

Intestinal single-cell suspensions were isolated from fresh endoscopic biopsies as previously described[5]. Briefly, tissues were collected in Hank's balanced salt solution (HBSS, ThermoFisher) after the endoscopy. Biopsies were treated with 10 mL of HBSS containing 1 mM ethylenediaminetetraacetic acid (EDTA, J.T.Baker) under rotation for 2 × 45 minutes at 37°C to separate the epithelium from the lamina propria. To obtain single cells from the lamina propria, biopsies were subsequently washed with HBSS and incubated with 5 mL of a collagenase mix containing Iscove's Modified Dulbecco's Media (IMDM) (Lonza) with 2% Fetal Calf Serum (FCS) (Bodinco), 1,000U/mL collagenase IV (Worthington), and 10 mg/mL DNAse I grade II (Roche Diagnostics) for 1.5 hours at 37°C. Cells isolated from both the epithelium and lamina propria were then together filtered through a 70 µm cell strainer and collected by centrifugation. To get rid of dead cells, the pellets were then incubated with 10 mg/mL DNase I in 5 ml 2% FCS/IMDM and filtered through a 30 µm cell strainer. The single-cell suspensions were collected after centrifugation and resuspended in IMDM complete medium supplemented with 2 mM L-glutamine (Lonza), 10% human serum, 100 U/mL Penicillin-Streptomycin (ThermoFisher), 0.25 ug/ml

Amphotericin B (Gibco merk), 100 µg/ml Normocin (InvivoGen) at 4°C for future steps. This whole process from patient to cell suspension takes about 4.5 hours.

PBMCs were isolated from up to 8mL freshly drawn heparin anticoagulated blood using Ficoll-Paque™ density-gradient centrifugation. Isolated cells were washed with phosphate-buffered saline (PBS), counted, and 1 million cells were stored in 20% FCS/RPMI at 4°C for future steps.

T-cell activation

Non-tissue culture-treated plates (24 well, flat Bottom, Corning) were incubated with 4 µg/mL goat anti-mouse IgG (Jackson ImmunoResearch) at 4°C overnight in PBS and subsequently with 2.5 µg/mL α-CD3 (clone Hit3a, ThermoFisher) at 37 °C for 3 hours in PBS. The fresh intestinal single cells and PBMCs were seeded in the α-CD3 pre-coated plates with α-CD28 (clone CD28.2, ThermoFisher) in complete medium for 6 h at 37 °C. In cohort 1, Brefeldin A (1:1000, Sigma-Aldrich) was added for the final 5 hours; in cohort 2, monensin (1:1500, BD GolgiStop™) was added for the final 3 h. Monensin and brefeldin A were used in separate settings with comparable cytokine retention efficiency. Data from both experiments were combined.

Full-spectrum flow cytometry

Briefly, for surface staining, cells were incubated with fluorochrome-conjugated antibodies, human Fc block and monocyte block (BioLegend) for 30 min at 4 °C in 0.5%/PBS. Cells were then fixed/permeabilized using Foxp3/Transcription Factor Staining Buffer Set (ThermoFisher). Intracellular staining for transcription factors, cytokines and Ki67 was performed for 45 min at 4 °C in Perm Wash Buffer (ThermoFisher). Samples were measured on 5-laser Aurora (Cytek), and unmixed with single stained controls on PBMC or UltraComp eBeads (ThermoFisher) on SpectroFlo platform (Cytek). Unstained reference controls used to subtract autofluorescence were paired to their corresponding fully stained samples. Sample processing, staining and measurement for phenotypic identification were performed within the same day; cells for cytokines profile identification were fixed and stored at 4 °C in 0.5%/PBS overnight, subsequently stained with intracellular antibodies and measured at the second day. To account for technical variation, reference samples of PBMCs and tonsillar mononuclear cells from identical donor were included in every mass cytometry experiment. Data was analyzed with FlowJo software version 10 (Tree Star Inc) and OMIQ online platform (https://www.omiq.ai/, Inc.,

Santa Clara, CA, USA). All antibodies used are listed in Supplementary Table 1 and 2.

Multispectral immunofluorescence and microscopy

Freshly obtained biopsies were formalin-fixed and paraffin-embedded by the Department of Pathology at LUMC. 4 µm sections were cut using a microtome, mounted on silane-coated slides, and dried overnight at 37 °C. Sections were deparaffinated using a xylol followed by decreasing concentrations of ethanol. For antigen retrieval, sections were boiled in 1x Tris-EDTA buffer (10 mM, pH 9) for 10 min and allowed to cool down for ± 60 min. Each sections were blocked by Superblock (Thermofisher) for 10 min at room temperature (rT). Excess superblock was removed and replaced with diluted primary antibody, followed by a 1 hour incubation at rT. After primary incubation, tyramide signal amplification was performed with poly-HRP (immunologic) for 10 min at rT, followed by incubation with Opal (Akoya Biosciences) for 10 min in the dark at rT according to manufacturer's instructions. Next, sections were boiled in 1x citrate buffer (10 mM, pH 6) for 15 min to permit further staining cycles. The staining sequence followed the order of CD3, E-cadherin, CD103, CD8 and CD4 (antibodies used are listed in Supplementary Table 3). Lastly, the sections were incubated with 1 µM DAPI for 15 min at rT in the dark for nuclear counterstaining, and mounted with using ProLong Gold Antifade Reagent (CAT#9071, CST). For each biopsies, five different tissue sections were imaged at 20× magnification with the Vectra 3.0 Automated Quantitative Pathology Imaging System (Perkin Elmer). Qupath was used for image analysis and spectral separation of dyes, by using spectral libraries defined with single-marker immunofluorescence detection.

Integrated data analysis

Dimensionality reduction (opt-SNE) on $CD3^+$ T cells data was performed on OMIQ following the R package "PeacoQC" to perform the automated cleaning of anomalies and arcsinh-transformed with cofactor manually; scaled $CD4^+$ memory T cells and CD8α T cells were exported from OMIQ and then performed by t-SNE computation on Cytosplore software using the default settings. Concerning cellular heterogeneity and large variability in cell abundance, samples with excessive cell numbers were downsampled to 1,000 cells each to ensure comparability across groups. Wishbone trajectory analysis of IBD-associated clusters were conducted in OMIQ, with CD4-13 cluster as starting point. PCA of the samples for cell cluster frequencies was performed using the R-package 'pca3d', where the

centroid for each patient group is plotted in a scatter plot. The R package 'corrplot' was used to calculate the correlation networks of cell frequencies of the identified cell subsets.

Statistics

Data were presented as median and interquartile range. Patient group comparisons were performed with two-tailed Mann-Whitney U tests or two-tailed Kruskal–Wallis's test with Dunn's test for multiple comparisons, as appropriate (GraphPad Prism 10). Linear Mixed-effects model was used to account for stimulation effects within each inflammation group (Fig. 5 A-C).

Acknowledgments

We thank all the patients for participating in this study. We thank all gastroenterologists and nurses for performing endoscopies and obtaining patients materials. We thank Zhixian Wang and Oscar R. J. van Hengel for valuable contributions to data analysis and programming. We thank Yizhi Wang for the help in tissue processing. We thank Zheng Li and Noel de Miranda from Department of Pathology for kindly help in histological staining and analysis. We thank Yanling Xiao for providing conceptual advice and scientific insight. In addition, we thank groupmates for insightful discussions and assistance with experiments and all the operators in the Flow Cytometry Core Facility of the LUMC for their technical assistance during measurements on Cytek Aurora.

Author contributions

QJ, FK, MFP, AM and VvU conceived the study and wrote the manuscript. AM, CRM and LO offered clinical advice and assisted in biopsies collection. QJ performed the experiments and analyzed the data. NG analyzed part of PBMC data. VM helped to perform the staining of tissue sections, TH provided conceptual input for trajectory analysis, and CL helped to perform the isolation of single cells.

Funding information

This research was supported by Leiden University Medical Center (QJ, CL, LO, FK, AM, VvU, MFP). VvU was supported by HORIZON-MSCA-PF (101109788), MFP and FK were supported by the collaboration project TIMID (LSHM18057-SGF) financed by the PPP allowance made available by Top Sector Life

Sciences & Health to Samenwerkende Gezondheidsfondsen (SGF) to stimulate public-private partnerships and co-financing by health foundations that are part of the SGF.

Conflict of interest statement

The authors declare that the research was conducted in the absence of any commercial or financial relationships that could be construed as a potential conflict of interest.

Reference

1. Khor B, Gardet A, Xavier RJ. Genetics and pathogenesis of inflammatory bowel disease. *Nature* 2011; **474**(7351)**:** 307–317.

2. de Souza HS, Fiocchi C. Immunopathogenesis of IBD: current state of the art. *Nat Rev Gastroenterol Hepatol* 2016; **13**(1)**:** 13–27.

3. Turner D, Ricciuto A, Lewis A, D'Amico F, Dhaliwal J, Griffiths AM *et al.* STRIDE-II: An Update on the Selecting Therapeutic Targets in Inflammatory Bowel Disease (STRIDE) Initiative of the International Organization for the Study of IBD (IOIBD): Determining Therapeutic Goals for Treat-to-Target strategies in IBD. *Gastroenterology* 2021; **160**(5)**:** 1570–1583.

4. Maaser C, Sturm A, Vavricka SR, Kucharzik T, Fiorino G, Annese V *et al.* ECCO-ESGAR Guideline for Diagnostic Assessment in IBD Part 1: Initial diagnosis, monitoring of known IBD, detection of complications. *J Crohns Colitis* 2019; **13**(2)**:** 144–164.

5. Atreya R, Neurath MF. Biomarkers for Personalizing IBD Therapy: The Quest Continues. *Clin Gastroenterol Hepatol* 2024; **22**(7)**:** 1353–1364.

6. Maloy KJ, Powrie F. Intestinal homeostasis and its breakdown in inflammatory bowel disease. *Nature* 2011; **474**(7351)**:** 298–306.

7. Ma Z, Wang Z, Cao J, Dong Y, Chen Y. Regulatory roles of intestinal CD4(+) T cells in inflammation and their modulation by the intestinal microbiota. *Gut Microbes* 2025; **17**(1)**:** 2560019.

8. Shale M, Schiering C, Powrie F. CD4(+) T-cell subsets in intestinal inflammation. *Immunol Rev* 2013; **252**(1)**:** 164–182.

9. Sheridan BS, Lefrancois L. Regional and mucosal memory T cells. *Nat Immunol* 2011; **12**(6)**:** 485–491.

10. Saravia J, Chapman NM, Chi H. Helper T cell differentiation. *Cellular & Molecular Immunology* 2019; **16**(7)**:** 634–643.

11. DuPage M, Bluestone JA. Harnessing the plasticity of CD4(+) T cells to treat immune-mediated disease. *Nat Rev Immunol* 2016; **16**(3)**:** 149–163.

12. Wang L, Liang Y, Zhao C, Ma P, Zeng S, Ju D *et al.* Regulatory T cells in homeostasis and disease: molecular mechanisms and therapeutic potential. *Signal Transduct Target Ther* 2025; **10**(1)**:** 345.

13. Casalegno Garduno R, Dabritz J. New Insights on CD8(+) T Cells in Inflammatory Bowel Disease and Therapeutic Approaches. *Front Immunol* 2021; **12:** 738762.

14. Corridoni D, Antanaviciute A, Gupta T, Fawkner-Corbett D, Aulicino A, Jagielowicz M *et al.* Single-cell atlas of colonic CD8(+) T cells in ulcerative colitis. *Nat Med* 2020; **26**(9)**:** 1480–1490.

15. Gasparetto M, Payne F, Nayak K, Kraiczy J, Glemas C, Philip-McKenzie Y *et al.* Transcription and DNA Methylation Patterns of Blood-Derived CD8+ T Cells Are Associated With Age and Inflammatory Bowel Disease But Do Not Predict Prognosis. *Gastroenterology* 2021; **160**(1)**:** 232–244.e237.

16. van Unen V, Ouboter LF, Li N, Schreurs M, Abdelaal T, Kooy-Winkelaar Y *et al.* Identification of a Disease-Associated Network of Intestinal Immune Cells in Treatment-Naive Inflammatory Bowel Disease. *Front Immunol* 2022; **13:** 893803.

17. van Unen V, Hollt T, Pezzotti N, Li N, Reinders MJT, Eisemann E *et al.* Visual analysis of mass cytometry data by hierarchical stochastic neighbour embedding reveals rare cell types. *Nat Commun* 2017; **8**(1)**:** 1740.

18. Li N, van Unen V, Hollt T, Thompson A, van Bergen J, Pezzotti N *et al.* Mass cytometry reveals innate lymphoid cell differentiation pathways in the human fetal intestine. *J Exp Med* 2018; **215**(5)**:** 1383–1396.

19. Godfrey DI, Uldrich AP, McCluskey J, Rossjohn J, Moody DB. The burgeoning family of unconventional T cells. *Nat Immunol* 2015; **16**(11)**:** 1114–1123.

20. Mayassi T, Barreiro LB, Rossjohn J, Jabri B. A multilayered immune system through the lens of unconventional T cells. *Nature* 2021; **595**(7868)**:** 501–510.

21. Xu B, Ji J, Ma L, Wang C, Pang L, Song Q *et al.* gammadeltaT Cells in IBD: Beneficial or Detrimental? *Immunology* 2025; **176**(3)**:** 337–348.

22. Lo Presti E, Mocciaro F, Mitri RD, Corsale AM, Di Simone M, Vieni S *et al.* Analysis of colon-infiltrating gammadelta T cells in chronic inflammatory bowel disease and in colitis-associated cancer. *J Leukoc Biol* 2020; **108**(2)**:** 749–760.

23. Dart RJ, Zlatareva I, Vantourout P, Theodoridis E, Amar A, Kannambath S *et al.* Conserved gammadelta T cell selection by BTNL proteins limits progression of human inflammatory bowel disease. *Science* 2023; **381**(6663)**:** eadh0301.

24. Liao CM, Zimmer MI, Wang CR. The functions of type I and type II natural killer T cells in inflammatory bowel diseases. *Inflamm Bowel Dis* 2013; **19**(6)**:** 1330–1338.

25. Fang Y, Chen Y, Niu S, Lyu Z, Tian Y, Shen X *et al.* Biological functions and therapeutic applications of human mucosal-associated invariant T cells. *J Biomed Sci* 2025; **32**(1)**:** 32.

26. Hu Y, Yang Y, Li Y, Zhang Q, Zhang W, Jia J *et al.* Th17/Treg imbalance in inflammatory bowel disease: immunological mechanisms and microbiota-driven regulation. *Front Immunol* 2025; **16:** 1651063.

27. Ohara D, Takeuchi Y, Hirota K. Type 17 immunity: novel insights into intestinal homeostasis and autoimmune pathogenesis driven by gut-primed T cells. *Cell Mol Immunol* 2024; **21**(11)**:** 1183–1200.

28. Schmitt H, Neurath MF, Atreya R. Role of the IL23/IL17 Pathway in Crohn's Disease. *Front Immunol* 2021; **12:** 622934.

29. Dziegielewski C, Yuan Y, Ma C, Boland BS, Chang JT, Syal G *et al.* IL-23p19 Antagonists vs Ustekinumab for Treatment of Crohn's Disease: A Meta-Analysis of Randomized Controlled Trials. *Am J Gastroenterol* 2025; **120**(10)**:** 2260–2267.

30. Feagan BG, Sandborn WJ, Gasink C, Jacobstein D, Lang Y, Friedman JR *et al.* Ustekinumab as Induction and Maintenance Therapy for Crohn's Disease. *N Engl J Med* 2016; **375**(20)**:** 1946–1960.

31. Moschen AR, Tilg H, Raine T. IL-12, IL-23 and IL-17 in IBD: immunobiology and therapeutic targeting. *Nat Rev Gastroenterol Hepatol* 2019; **16**(3)**:** 185–196.

32. Park E, Ciofani M. Th17 cell pathogenicity in autoimmune disease. *Exp Mol Med* 2025; **57**(9)**:** 1913–1927.

33. Xu H, Agalioti T, Zhao J, Steglich B, Wahib R, Vesely MCA *et al.* The induction and function of the anti-inflammatory fate of T(H)17 cells. *Nat Commun* 2020; **11**(1)**:** 3334.

34. Cheng H, Nan F, Ji N, Ma X, Zhang J, Liang H *et al.* Regulatory T cell therapy promotes TGF-beta and IL-6-dependent pro-inflammatory Th17 cell generation by reducing IL-2. *Nat Commun* 2025; **16**(1)**:** 7644.

35. Allegretti JR, Mitsialis V, Canavan JB, Low-Dose ILUCSG, Snapper SB. Low-Dose Interleukin 2 for the Treatment of Moderate to Severe Ulcerative Colitis. *Gastroenterology* 2023; **165**(2)**:** 492–495 e492.

36. Cui Y, David M, Bouchareychas L, Rouquier S, Sajuthi S, Ayrault M *et al.* IL23R-Specific CAR Tregs for the Treatment of Crohn's Disease. *J Crohns Colitis* 2025; **19**(3).

37. Sollid LM. Tolerance-inducing therapies in coeliac disease - mechanisms, progress and future directions. *Nat Rev Gastroenterol Hepatol* 2024; **21**(5)**:** 335–347.

38. Yokoi T, Murakami M, Kihara T, Seno S, Arase M, Wing JB *et al.* Identification of a unique subset of tissue-resident memory CD4(+) T cells in Crohn's disease. *Proc Natl Acad Sci U S A* 2023; **120**(1)**:** e2204269120.

39. Lamb CA, O'Byrne S, Keir ME, Butcher EC. Gut-Selective Integrin-Targeted Therapies for Inflammatory Bowel Disease. *J Crohns Colitis* 2018; **12**(suppl_2)**:** S653–S668.

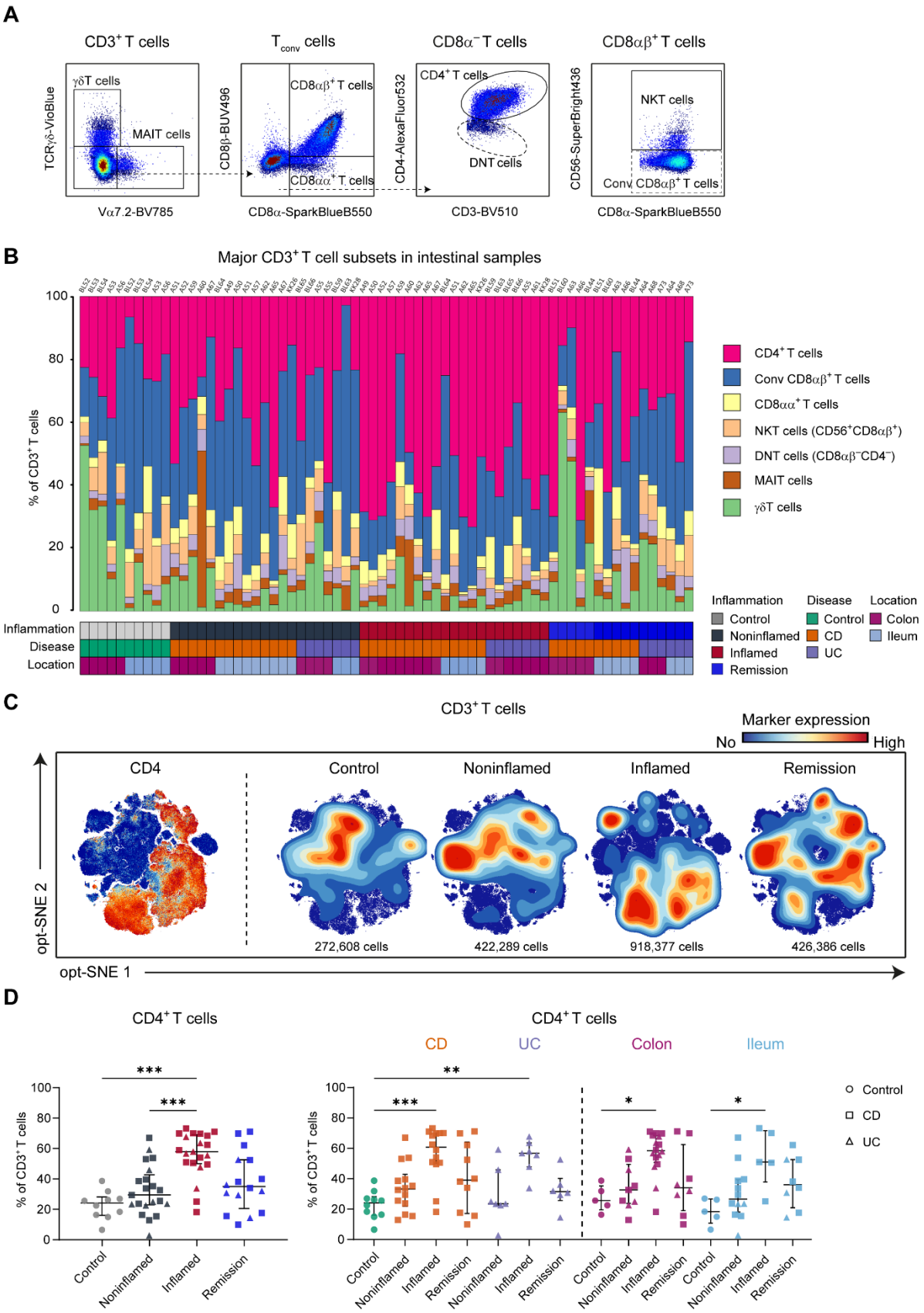

Fig. 1. CD4⁺ T cells act as major contributors to the amplification of inflammatory processes within the tissue. (A), Bivariate plots showing the gating strategy to identify 7 major CD3⁺ T-cell subsets in

intestinal samples, including $CD4^+$ T, conventional $CD8\alpha\beta^+$ T, $CD8\alpha\alpha^+$ T, NKT ($CD56^+CD8\alpha\beta^+$), Double Negative (DN, $CD8ab^-CD4^-$), MAIT and γδ T cells. **(B)**, Bar graph showing cell frequencies of 7 major $CD3^+$ T-cell subsets. Heatmaps showing clinical metadata stratified for disease state (controls: patients with non-autoimmune disease; noninflamed: endoscopic noninflamed segment in IBD patient; inflamed: currently endoscopic active disease; remission: segment in endoscopic remission), disease subtype (control, CD and UC) and intestinal location (colon and ileum). **(C)**, opt-SNE embedding of the collective $CD3^+$ T cells derived from 68 samples plots displaying CD4 expression in intestinal $CD3^+$ T cells. Density maps showing the density of cells stratified for disease state. **(D)**, The frequencies of $CD4^+$ T cells stratified for disease state, disease subtype and intestinal location, as percentage of total $CD3^+$ T cells. Error bars indicate the median with interquartile range. *$p \leq 0.05$, **$p \leq 0.01$, ***$p \leq 0.001$, Kruskal–Wallis test with Dunn's test for multiple comparisons.

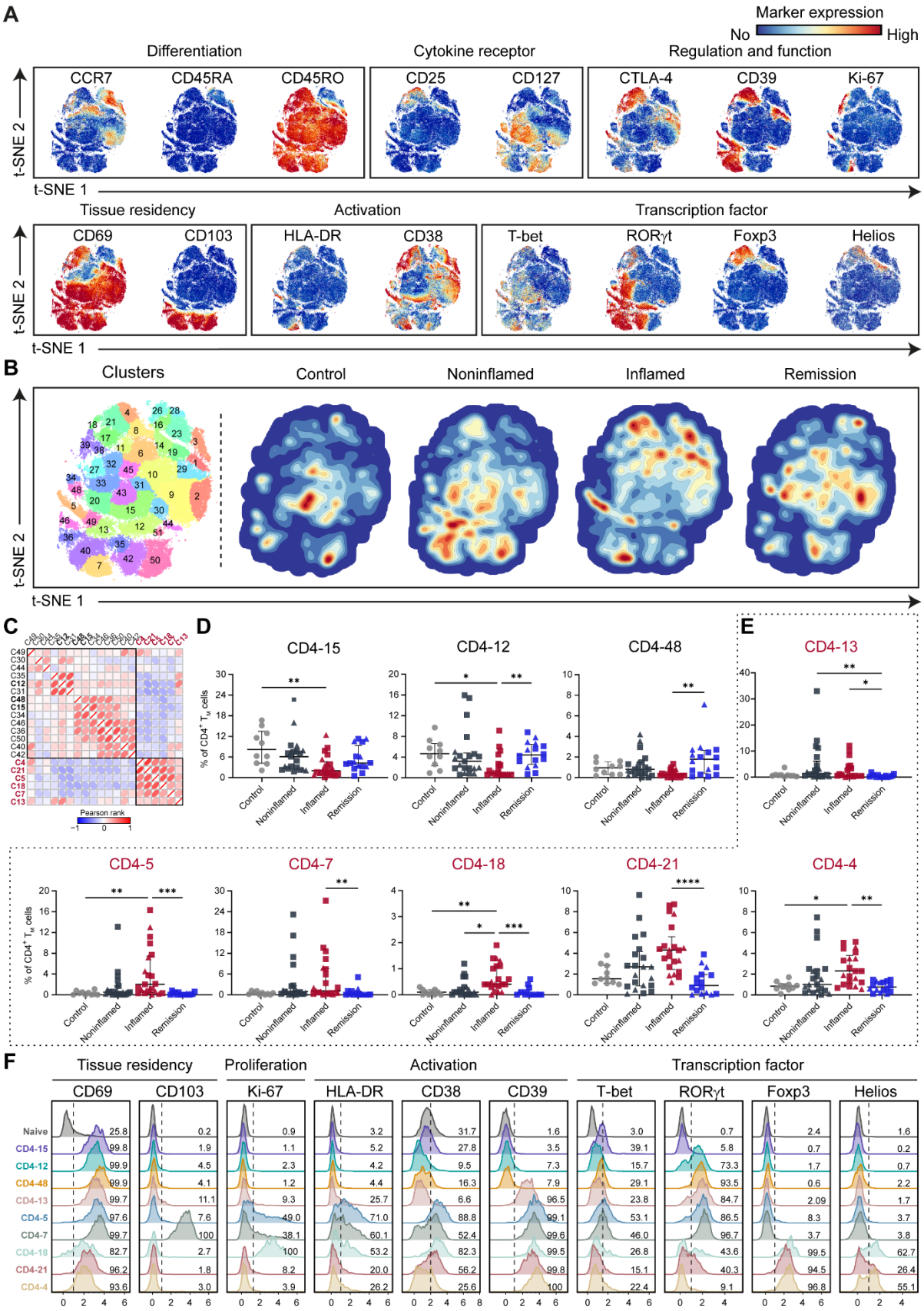

Fig. 2. The Inflammation niche facilitates the development of distinct heterogeneous clusters. (A), t-SNE plots embedding of 65,732 intestinal CD4⁺ memory T cells colored for the expression values of the

indicated markers. Samples were downsampled to 1,000 cells if applicable. **(B)**, t-SNE plot showing cluster partitions in different colors. Density maps showing the density of cells stratified for disease state. **(C)**, Correlation matrix of clusters that exhibited clear trends during inflammation based on Pearson correlation coefficients. Hierarchical clustering of correlations indicated by two black squares. **(D-E)**, Dot plots showing frequencies of indicated clusters stratified for disease state. Error bars indicate the median with interquartile range. *$p \leq 0.05$, **$p \leq 0.01$, ***$p \leq 0.001$, Kruskal–Wallis test with Dunn's test for multiple comparisons. **(F)**, Overlay of $CD4^+$ naive T cells (random selection of 1,000 naive cells from 68 samples) and IBD-associated clusters (derived from **2D-E**) on histograms illustrating the expression patterns of markers related to tissue residency (CD69 and CD103), cell proliferation (Ki-67), activation (HLA-DR, CD38 and CD39) and transcription factors (T-bet, RORγt, Foxp3 and Helios).

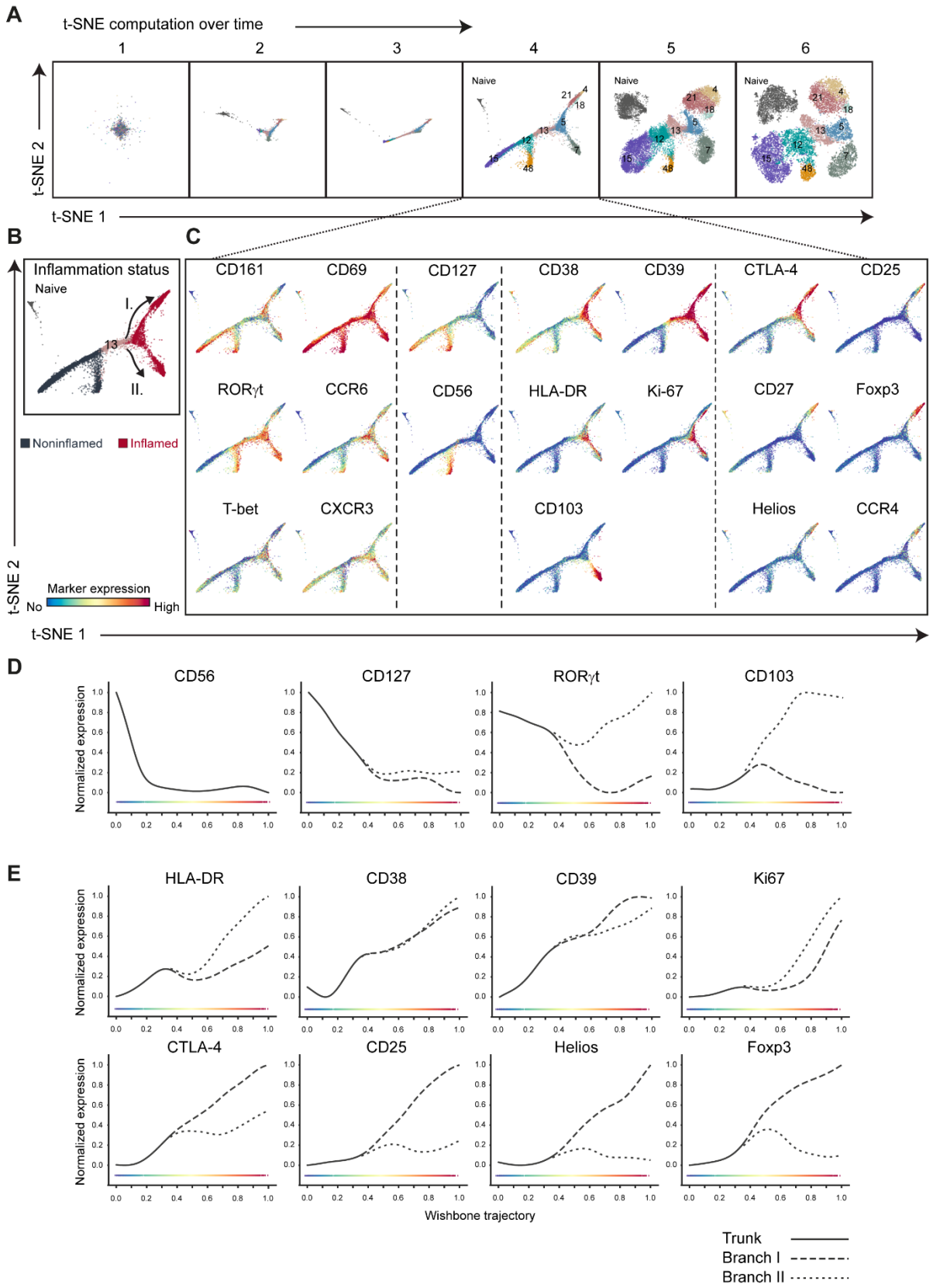

Fig. 3. Potential differentiation trajectories of CD4 clusters in development of inflammation. (A), t-SNE embeddings of CD4⁺ naive T cells (random selection of 1,000 naive cells from 68 samples) and 9

IBD-associated CD4 clusters derived from **Fig. 2D-F**, showing single cells at six stages over the course of the t-SNE computation. Colors represent cluster partitions as described in **Fig. 2F**. **(B-C)**, t-SNE embeddings at stage 4 of the optimization phase as described in **3A**. Arrows in **B** showing 2 potential trajectories along the process of inflammation, and markers with different expression patterns in the two branches are shown in **C**. **(D-E)**, line plots generated by Wishbone (trajectory 0-1.0) showing the changes in normalized expression of indicated markers along bifurcating developmental trajectories.

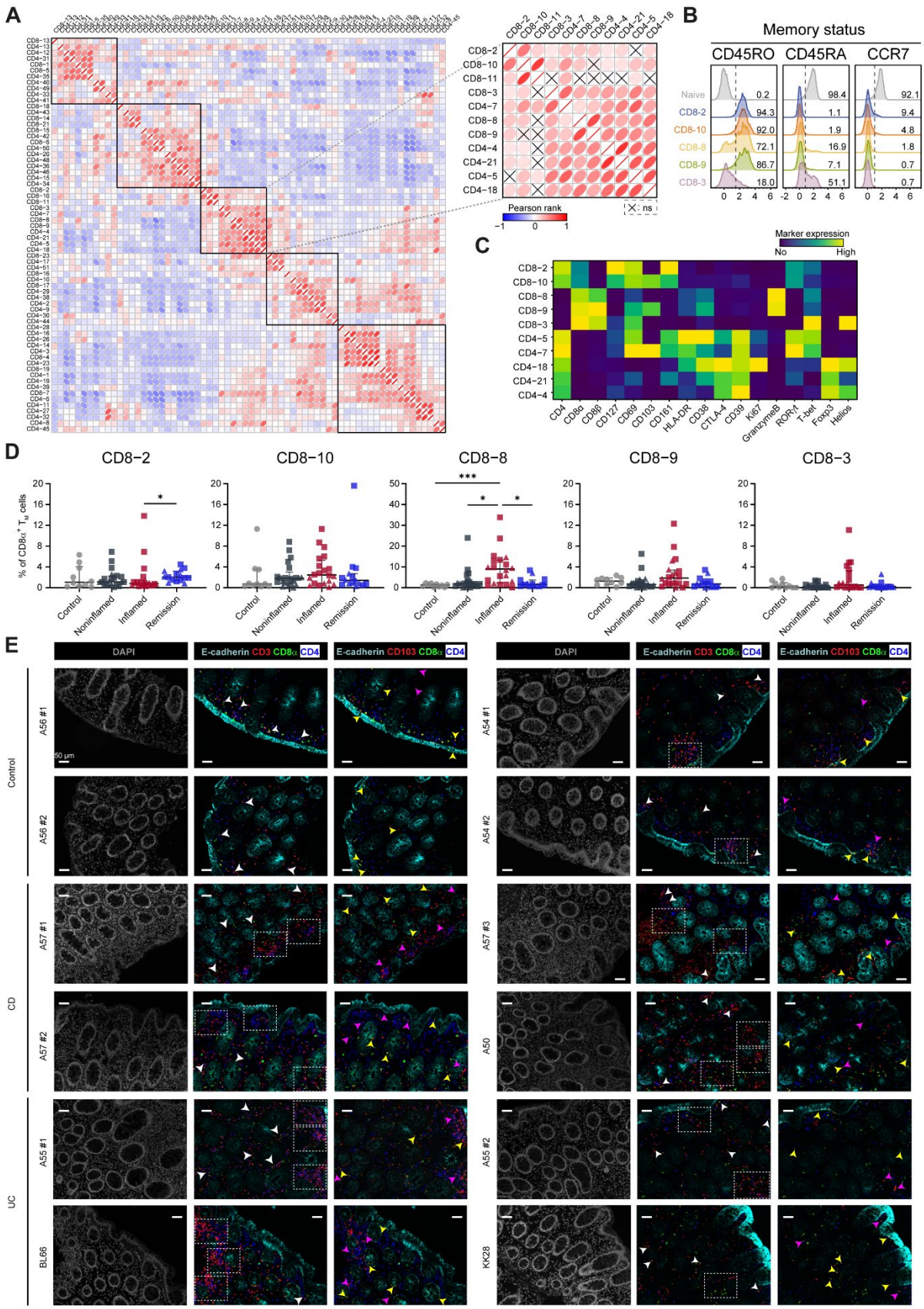

Fig. 4. CD4–CD8 T cell crosstalk in the lamina propria. (A), Pearson rank-based correlation matrix showing pairwise relationships among all memory CD4 clusters and CD8 clusters based on cell

percentages (of total memory $CD4^+$ and $CD8\alpha^+$ T cells). Magnified view of the third network presenting the statistical evaluation of inter-cluster correlations. “ns” denotes non-significant correlations. **(B)**, Overlay histogram showing significantly correlated clusters and naive clusters with CD45RO, CD45RA and CCR7 expression profiles. **(C)**, Heatmap showing median marker expression values of inflammation-associated CD4 clusters and CD8 clusters identified from **(A)**. **(D)**, The frequencies of CD8 clusters stratified for disease state, as percentage of total $CD8\alpha^+$ T cells. Error bars indicate the median with interquartile range. *$p \leq 0.05$, **$p \leq 0.01$, ***$p \leq 0.001$, Kruskal–Wallis test with Dunn’s test for multiple comparisons. **(E)**, Representative images of the immunofluorescence microscopic detection of CD103 positive $CD4^+$ and $CD8\alpha^+$ T cells in control, CD and UC samples, showing E-cadherin (colored in cyan), CD3 (colored in red), CD8α (colored in green), CD4 (colored in blue), and DAPI (colored in grey) as nuclear counterstain. Regions of CD4-CD8 cell colocalization within each ROI are marked by white arrows. Yellow arrows: $CD3^+CD8\alpha^+CD103^+$ cells; magenta arrows: $CD3^+CD4^+CD103^+$ cells. Scale bar, 50 μm.

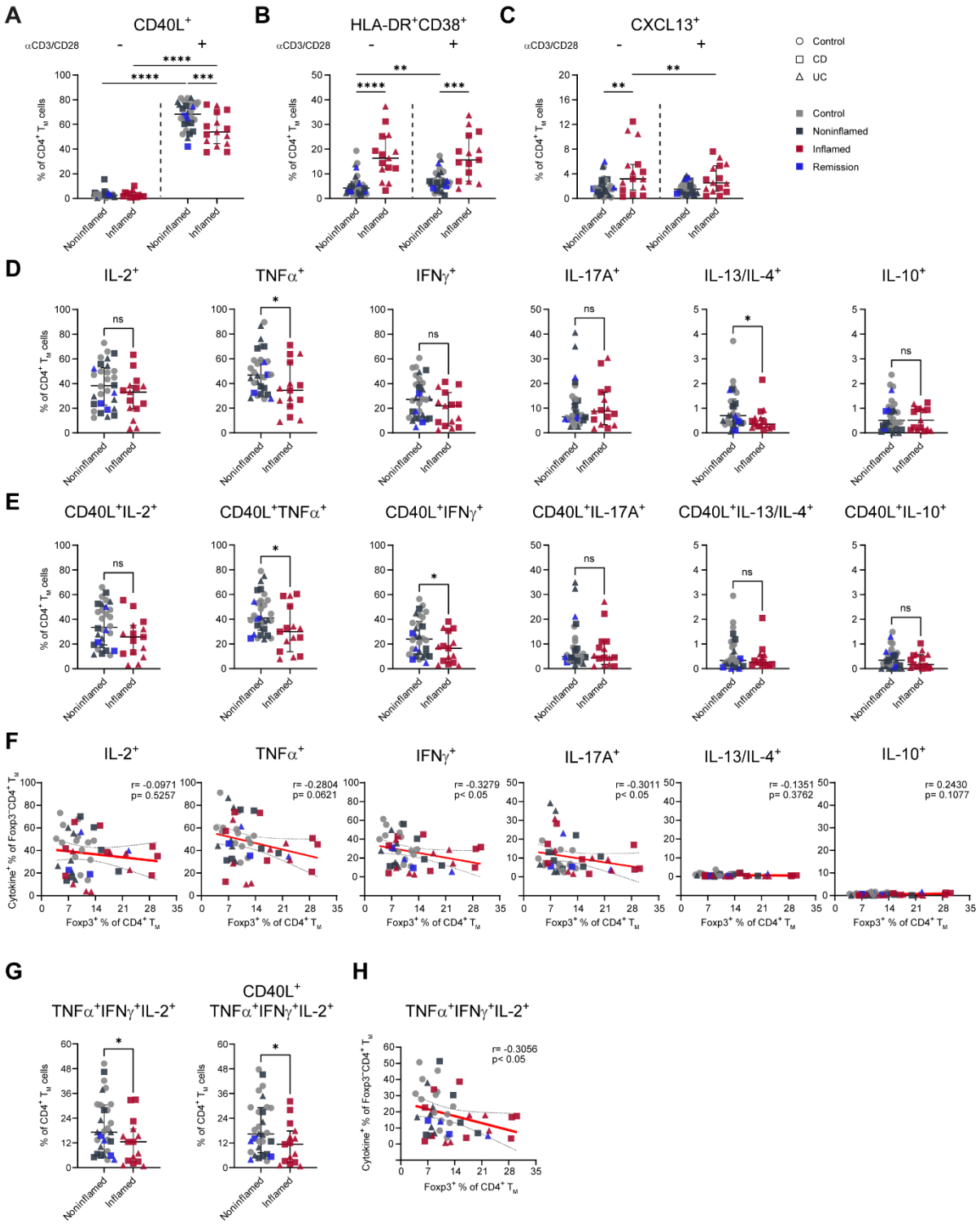

Fig. 5. Functional profiling of intestinal CD4⁺ memory T cells. The intestinal suspensions were treated with α-CD3 and α-CD28 for 6 hours. **(A–C)** The frequencies of CD40L⁺, HLA-DR⁺CD38⁺, and CXCL13⁺

cells in $CD4^+$ memory T cells before and after stimulation, compared between noninflamed and inflamed groups. **(D-E),** Intracellular expression of IL-2, TNFα, IFNγ, IL-17A, IL-13/IL-4 and IL-10 in total $CD4^+$ memory T cells **(D)** and the responsive ($CD40L^+$) memory T cells **(E)**, determined for noninflamed and inflamed groups by flow cytometry. **(F)**, Correlations between frequencies of $Foxp3^-$ $CD4^+$ memory T cells producing IL-2, TNFα, IFNγ, IL-17A, IL-13/IL-4, IL-10 and frequencies of $Foxp3^+$ $CD4^+$ memory T cells were assessed using simple linear regression. Spearman's rank correlation was used to determine correlation coefficients and *p* values. **(G),** The frequencies of $TNFα^+IFNγ^+IL\text{-}2^+$ cells in $CD4^+$ memory T cells and the responsive ($CD40L^+$) memory T cells, determined for noninflamed and inflamed groups by flow cytometry. **(H),** Correlation analysis showing the relationship between the frequencies of $Foxp3^-$ $CD4^+$ memory T cells producing TNFα, IFNγ and IL-2 simultaneously and $Foxp3^+$ $CD4^+$ memory T cells. Error bars indicate the median with interquartile range. "ns" denotes not significant, *$p \leq 0.05$, **$p \leq 0.01$, ***$p \leq 0.001$, Mann-Whitney test.

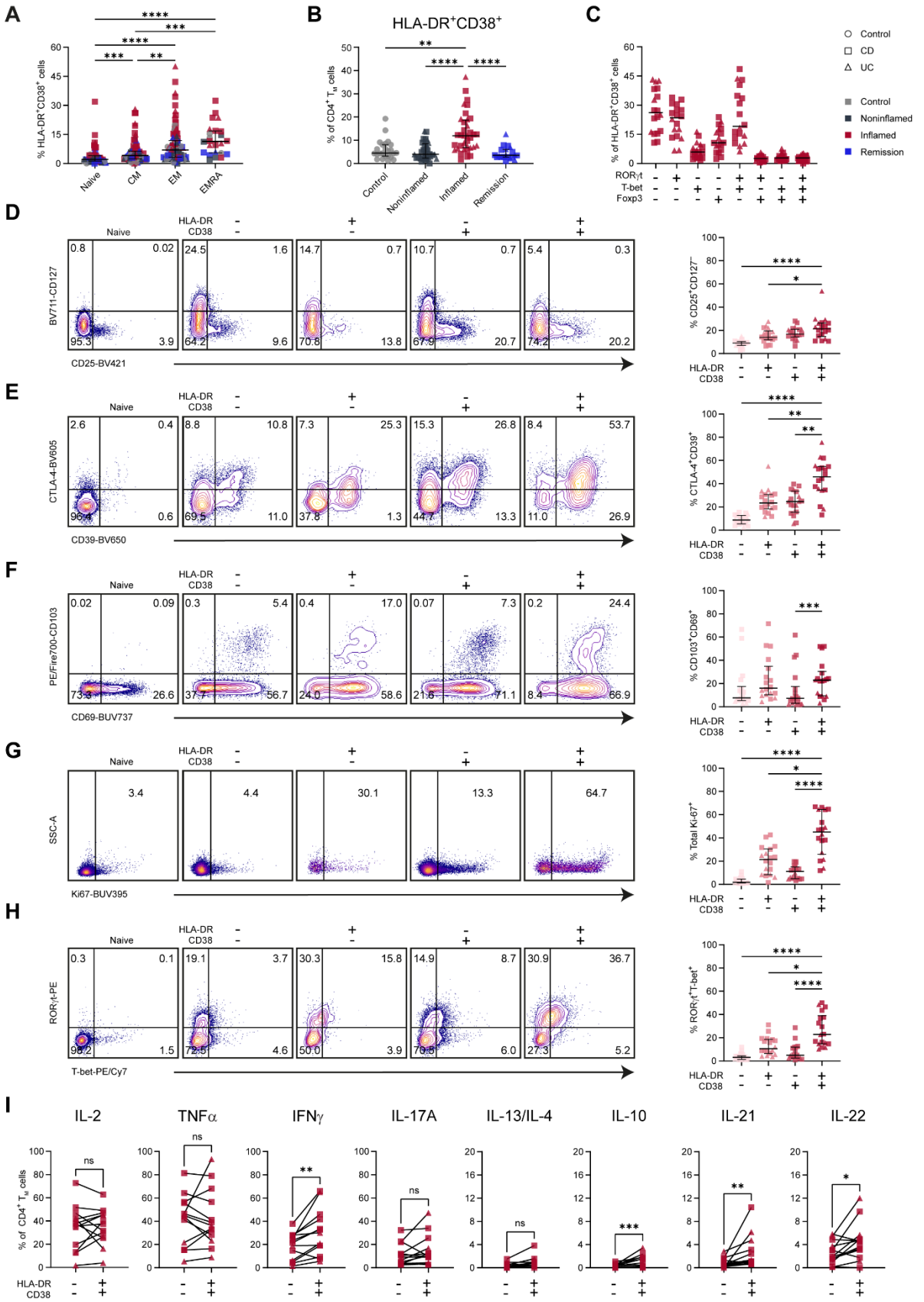

Fig. 6. The phenotypic characterizations and functional profile of IBD associated HLA-DR$^+$CD38$^+$ cells.

(A), Dot plots shows the percentage of double positive HLA-DR and CD38 cells in the naive, central

memory (CM), effector memory (EM) and terminally differentiated effector memory (EMRA) of $CD4^+$ T cells**. (B)**, The frequencies of double positive HLA-DR and CD38 cells stratified for disease state, as percentage of total $CD4^+$ memory T cells. **(C)**, Distribution of cells co-expressing various combinations of the three transcription factors (RORγ, T-bet and Foxp3) among HLA-DR^+ $CD38^+$ $CD4^+$ memory T cells. **(D-H)**, The frequencies of $CD25^+CD127^+$, CTLA-4^+CD39^+, $CD103^+CD69^+$, Ki-67^+ and $ROR\gamma^+$T-bet^+ cells compared among four groups defined by HLA-DR (positive or negative) and CD38 (positive or negative) expression, shown in biaxial plots (data from one representative experiment, compared by naïve cells, left) and dot plots (right). **(I)**, The frequencies of IL-2, TNFα, IFNγ, IL-17A, IL-13/IL-4 and IL-10 were compared between HLA-DR^-CD38^- and HLA-DR^+CD38^+ populations, as percentage of total $CD4^+$ memory T cells. Error bars indicate the median with interquartile range. *$p \leq 0.05$, **$p \leq 0.01$, ***$p \leq 0.001$, "ns" denotes not significant, Kruskal–Wallis test with Dunn's test for multiple comparisons.